Supplementary Information for

Direct Observation of Xe and Kr Adsorption in a Xe-selective Microporous Metal Organic Framework

Xianyin Chen[1], Anna M. Plonka[2], Debasis Banerjee[3], Rajamani Krishna[4], Herbert T. Schaef [3], Sanjit Ghose[5], Praveen K. Thallapally[3,*] and John B. Parise[1,2,5*]

[1]Department of Chemistry, Stony Brook University, Stony Brook, NY 11794, USA
[2]Department of Geosciences, Stony Brook University, Stony Brook, NY 11794, USA
[3]Fundamental & Computational Science Directorate, Pacific Northwest National Laboratory, Richland, WA- 99352, USA
[4]Van't Hoff Institute for Molecular Sciences, University of Amsterdam, Science Park 904, 1098 XH Amsterdam, The Netherlands
[5]Photon Sciences, Brookhaven National Laboratory, Upton, NY 11973, USA

Correspondence to: john.parise@stonybrook.edu ; praveen.thallapally@pnnl.gov

Contents

I. Experimental Section

1. Synthesis Method

SBMOF-2:H_2O was synthesized under solvothermal conditions using Teflon-lined 23-mL Parr® stainless steel autoclaves. Starting materials include calcium chloride ($CaCl_2$, 96%, Acros-Organics), 1,2,4,5-Tetrakis(4-carboxyphenyl)benzene (TCPB) ($C_{34}H_{22}O_8$, Sigma Aldrich, 98%) and ethanol (95%, Fisher Scientific) and were used without further purification. A mixture of 0.25 mmoles of $CaCl_2$ (0.027g) and 0.05 mmoles of TCPB (0.03g) were dissolved in 12 gram of ethanol and stirred for 2 hours to achieve homogeneity. The resultant solution was heated at 373 K for 3 days. Colorless prism crystals were recovered as products and washed with ethanol. The water molecules in the structure come from the 95% ethanol solvent and adsorbed moisture in the $CaCl_2$ reactant. The yield was 50% based on the linker, 0.02g.

2. Structure of SBMOF-2:H_2O and SBMOF-2

As-synthesized SBMOF-2:H_2O crystallizes in triclinic crystal system, space group *P*-1. Calcium is coordinated to six oxygen atoms from six independent linkers, forming isolated CaO_6 octahedra, which are bridged by the carboxylic groups of the linker, resulting in a porous framework. The linker is coordinating to six calcium ions in a monodentate mode. Uncoordinated -OH groups on carboxylates in type-II channels leaves a tendency of forming hydrogen bonds along the aperture. H4 atom remains for charge balance of SBMOF-2:H_2O. (Figure S2)

Porous MOFs with calcium polyhedra have been reported as 3-D structures of edged shared polyhedra, corner shared calcium octahedral chain, edged shared tetramers, and 2-D edged shared polyhedral chain. To the best of our knowledge, SBMOF-2 is the first porous 3-D example of isolated CaO_6 octahedra connected by linkers.

3. Thermogravimetry Analysis

TGA data of SBMOF-2:H_2O and SBMOF-2 were collected using a STA 449 C Jupiter Netzsch Instrument. Powder samples were placed in alumina crucible and heated from 298 K to 1023 K with a heating rate of 10 K/min under N_2 atmosphere.

4. Xe/Kr Gas Loading and Adsorption Analysis

Fresh crystals of SBMOF-2:H_2O were activated at 513 K and hold in vacuum for 5 hours and then were placed in a three-neck flask with gas (Xe/Kr) flowing into the flask. After that, the crystals were coated with Paratone® oil, keeping gas flowing to maintain 1 atm of gas, and representative crystal was chosen for single crystal diffraction.

Xenon (Xe) and krypton (Kr) adsorption/desorption isotherms were measured using a Micromeritics ASAP 2020 volumetric adsorption analyzer. Powder samples were degassed offline at 513 K for 10 hours under dynamic vacuum (10-5 bar) before analysis, followed by degassing on the analysis port under vacuum, also at 513 K.

5. Single Crystal and Powder X-ray Crystallography

Representative crystals of fresh, activated and gases loaded samples suitable for single crystal X-ray diffraction were selected from the bulk and were mounted in Paratone® oil on CryoLoop®. Data for compounds SBMOF-2, SBMOF-2:Xe and SBMOF-2:Kr were collected with 1°ω-scans at 100 K (SBMOF-2:H_2O at room temperature) using a four-circle kappa Oxford Gemini diffractometer equipped with an Atlas detector (λ= 0.71073/1.54184Å) (Table S1). The raw intensity data were collected, integrated, and corrected for adsorption effects using CrysAlisPRO software. Data sets were corrected for absorption using a multi-scan method, and structures were solved by direct methods using SHELXS-97[1] and refined by full-matrix least squares on F^2 with SHELXL-97.[2] Atoms belonging to the framework were located first, and refined aniostropically. Hydrogen atoms were added to the structure model using geometrical constraints (HFIX command). After obtaining satisfactory model of the framework, gas

atoms (Xe, Kr) were located from Fourier difference map and refined anisotropically with the occupancy refined.

Electron density maps calculated from single crystal diffraction data indicate strong ordering of Xe and Kr inside the pores (Figure S11). Furthermore, in the case of Xe we ob-served a large difference between levels of electron density in channel-II vs. channel-I (17.7 vs. 12.2 e/Å3 indicating stronger affinity of Xe for polarizing –OH groups rather than phenyl rings. Electron density maps for the Kr-adduct indicate that Kr is not as strongly differentiated between type-II and -I channels (4.0 vs. 3.3 e/Å3).

To confirm phase purity PXRD data were collected using a Rigaku Ultima-IV diffractometer Cu Kα (λ = 1.5418 Å) with a range of $5° \leq 2\theta \leq 40°$ (scanning rate: 1°/min). The powder patterns so collected were consistent with those simulated based on structure models derived from single crystal data (Figure S5). Full details of the structure determinations have been deposited with Cambridge Crystallographic Data Center under reference numbers CCDC 1039468-1039471 (specifically CCDC 1039468, SBMOF-2:H_2O; CCDC 1039469, SBMOF-2; CCDC 1039470 SBMOF-2:Xe; CCDC 1039471, SBMOF-2:Kr), and are available free of charge from CCDC.

6. Breakthrough Experiments

For the breakthrough measurements 130 mg of SBMOF-2 was packed in a 6.35 cm long and 0.5-cm diameter column. The sample was activated at 513 K under flowing helium overnight. Pressurization of the 0.25" (6.35 mm) diameter column packed with SBMOF-2 was accomplished with a syringe pump (Teledyne ISCO) directly connected to the system through a series of 0.07 mm (ID) segments of tubing (PEEK) and valves. System pressure was maintained by coordinated adjustments to the syringe pump flow rate and the needle metering valve (Tescom). An inline pressure transducer was used to verify column pressure. The column was cooled to room temperature and a mixture of 5% Kr and 5% Xe and 90% N_2 was introduced with a flow rate of 1 ml/min at a total pressure of 20 psi (1.36 atm). Effluent gas chemistry was tracked with a Stanford Research residual gas analyzer (RGA). Masses (a.m.u.) corresponding to N_2 (28), Xe

(131) and Kr (84) were monitored throughout the experiments. The flow rate (1 ml/min) through the needle metering valve created a sampling pressure of 1.0 to 3.0 × 10^{-4} Torr in the RGA and was maintained throughout the experiments. Indications of Xe and Kr breaking through the column were indicated by an increase in the pressure for masses 131 and 84 respectively. (See Figure S12)

II. Calculations

7. Langmuir-Freundlich Fitting of Pure Component Isotherms

The experimentally measured loadings for Xe and Kr in SBMOF-2 were measured as a function of the absolute pressure at three different temperatures 278 K, 288 K, and 298 K.

The isotherm data were fitted with the Langmuir-Freundlich model.

$$q = q_{sat}\frac{bp^{v}}{1+bp^{v}} \quad (1)$$

with T-dependent parameter b

$$b = b_0 \exp\left(\frac{E}{RT}\right) \quad (2)$$

Table S2 provides the Langmuir-Freundlich fit parameters for adsorption of Xe and Kr in SBMOF-2. Figure S9 provides a comparison of the pure component isotherm data for (a) Xe, (b) Kr in SBMOF-2 with the fitted isotherms (shown by continuous solid lines) at 278 K, 288 K, and 298 K. The fits are good for both components at all three temperatures.

8. Isosteric Heat of Adsorption

The isosteric heat of adsorption, Q_{st}, defined as:

$$Q_{st} = RT^2\left(\frac{\partial \ln p}{\partial T}\right)_q \quad (3)$$

were determined using the pure component isotherm fits using the Clausius-Clapeyron equation. (Figure 2B)

9. IAST Calculation of Adsorption Selectivity and Uptake Capacities.

The selectivity of preferential adsorption of component 1 over component 2 in a mixture containing 1 and 2, perhaps in the presence of other components too, can be formally defined as:

$$S_{ads} = \frac{q_1/q_2}{p_1/p_2} \qquad (4)$$

In equation (4), q_1 and q_2 are the *absolute* component loadings of the adsorbed phase in the mixture. These component loadings are also termed the uptake capacities. In all the calculations to be presented below, the calculations of q_1 and q_2 are based on the use of the Ideal Adsorbed Solution Theory (IAST) of Myers and Prausnitz.[3]

10. Transient Breakthroughs in Fixed Bed Adsorbers

The separation of Xe/Kr mixtures is commonly carried out in fixed bed adsorbers in which the separation performance is dictated by a combination of three separate factors: (a) adsorption selectivity, (b) uptake capacity, and (c) intra-crystalline diffusivities of guest molecules within the pores. Transient breakthrough simulations are required for a proper evaluation of MOFs; the simulation methodology used in our work is described in earlier publications.[4,5]

The breakthrough characteristics for any component is essentially dictated by two sets of parameters: (a) The characteristic contact time $\frac{L}{v} = \frac{L\varepsilon}{u}$ between the crystallites and the surrounding fluid phase, and (b) $\frac{Đ_i}{r_c{}^2}$, that reflect the importance of intra-crystalline diffusion limitations. It is common to use the dimensionless time, $= \frac{tu}{L\epsilon}$, obtained by

dividing the actual time, *t*, by the characteristic time, $\frac{L\varepsilon}{u}$ when plotting simulated breakthrough curves.[4]

If the value of $\frac{D_i}{r_c^2}$ is large enough to ensure that intra-crystalline gradients are absent and the entire crystallite particle can be considered to be in thermodynamic equilibrium with the surrounding bulk gas phase at that time *t*, and position *z* of the adsorber. The assumption of thermodynamic equilibrium generally results in sharp breakthroughs for each component; sharp breakthroughs are desirable in practice because this would result in high productivity of pure products. When intra-crystalline diffusion effects are significant, the breakthrough has distended characteristics; this has the effect of reducing the productivity of pure gases. For Co Formate,[6] for example, intra-crystalline diffusion effects are particularly significant for Xe; this has the effect of reducing the productivity of pure Kr. (Figure S10)

Let us arbitrarily assume that the desired product Kr should have a purity corresponding to 1000 ppm Xe. Corresponding to this purity requirement we can determine the dimensionless breakthrough time, τ_{break}, at which the operation of the fixed bed needs to be stopped and regeneration started to recover pure Xe. From a material balance we can determine the productivity of Kr during the time interval 0 - τ_{break}. The productivities, expressed as mol of pure Kr produced per L of MOF are plotted in Figure S13 as a function of the dimensionless breakthrough time, τ_{break}. The MOF with the highest productivity is Ag@NiMOF-74. The productivity of SBMOF-2 is slightly below that of Co formate.

Notation:

b_A dual-Langmuir-Freundlich constant for species *i* at adsorption site A, $Pa^{-\nu i}$

b_B dual-Langmuir-Freundlich constant for species *i* at adsorption site B, $_iPa^{-\nu i}$

c_i molar concentration of species *i* in gas mixture, mol m^{-3}

c_{i0} molar concentration of species *i* in gas mixture at inlet to adsorber, mol m^{-3}

$Đ_i$ Maxwell-Stefan diffusivity, $m^2 s^{-1}$

L length of packed bed adsorber, m

n number of species in the mixture, dimensionless

p_i partial pressure of species *i* in mixture, Pa

p_t total system pressure, Pa

q_i component molar loading of species *i*, mol kg^{-1}

r_c radius of crystallite, m

R gas constant, 8.314 J mol^{-1} K^{-1}

t time, s

T absolute temperature, K

u superficial gas velocity in packed bed, m s^{-1}

Greek letters

ε voidage of packed bed, dimensionless

ρ framework density, kg m^{-3}

τ time, dimensionless

Subscripts

i referring to component *i*

t referring to total mixture

III. Figures and Tables

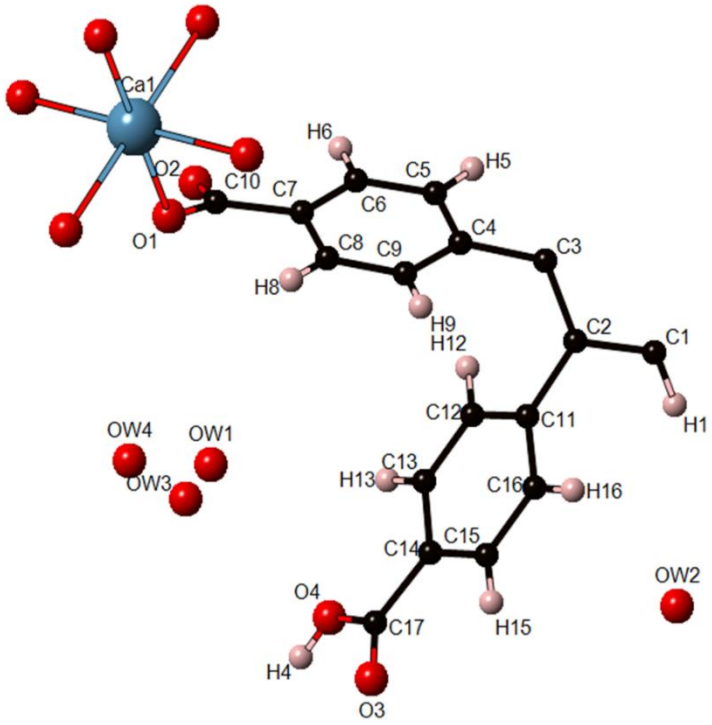

Figure S1. Asymmetric unit of SBMOF-2:H_2O, oxygen atoms coordinating to Ca were duplicated to fill the coordination sphere.

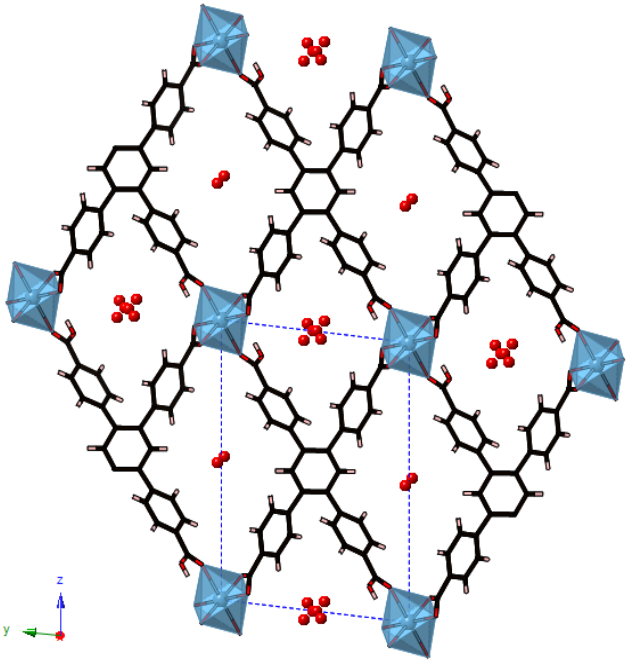

Figure S2. Structure of SBMOF-2:H_2O in [100]. (black sphere/stick represent carbon atoms/carbon bond, red sphere – oxygen, pink – hydrogen and blue – calcium).

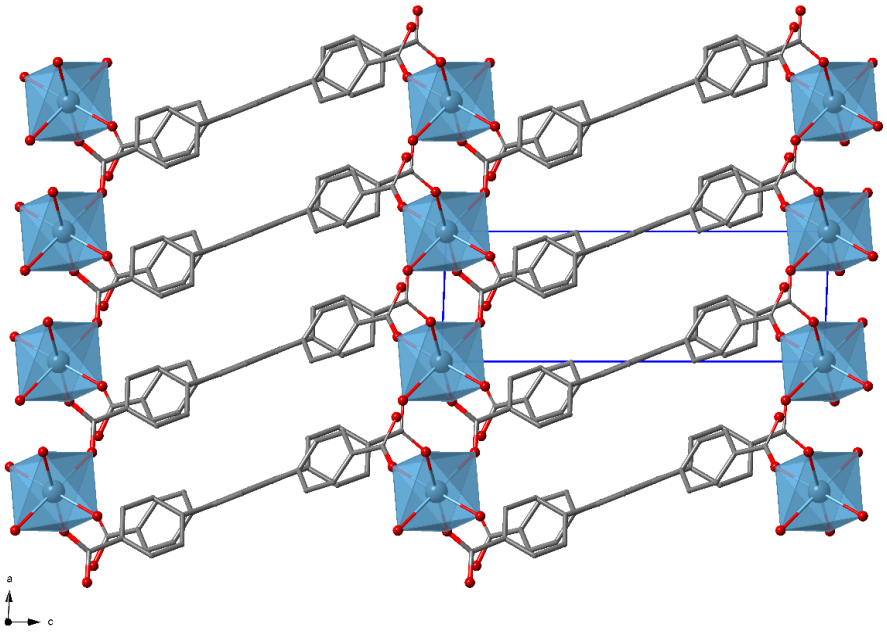

Figure S3. Structure of SBMOF-2:H2O in [010]. (black sphere/stick represent carbon atoms/carbon bond, red sphere – oxygen and blue – calcium. Hydrogen atoms are omitted for clarity)

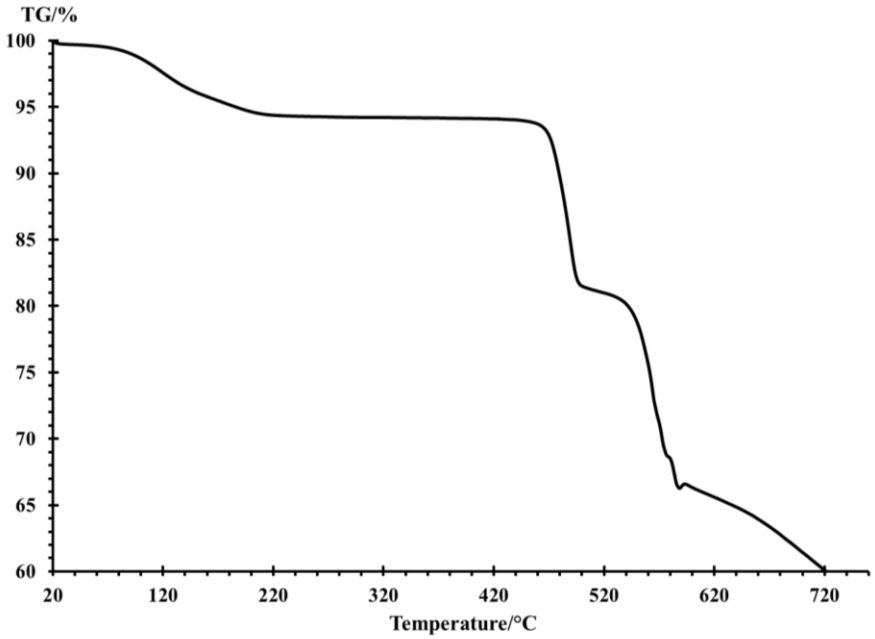

Figure S4. TGA plot of as-synthesized SBMOF-2:H_2O.

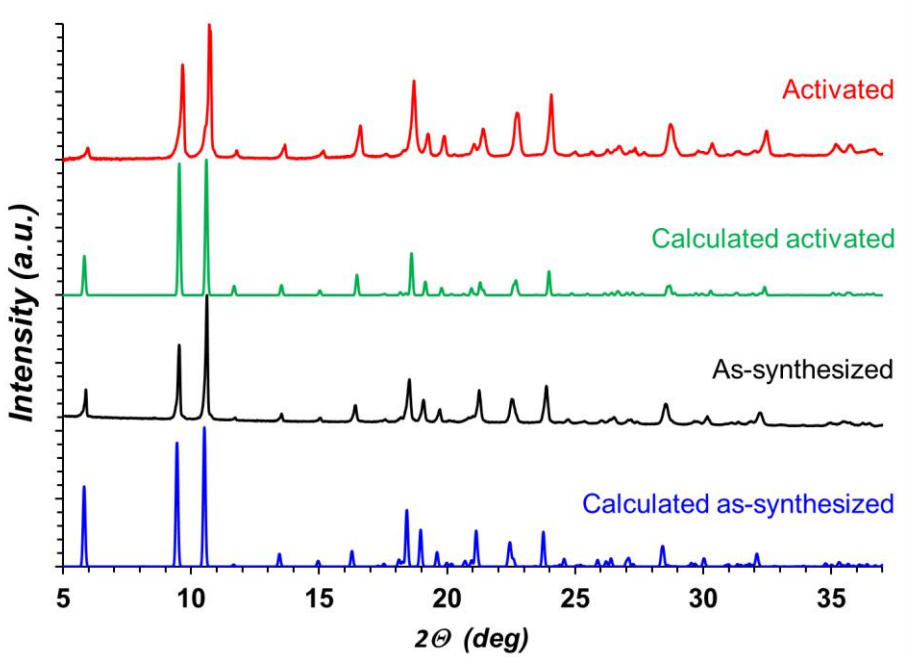

Figure S5. PXRD pattern of experimental and calculated, fresh and activated SBMOF-2.

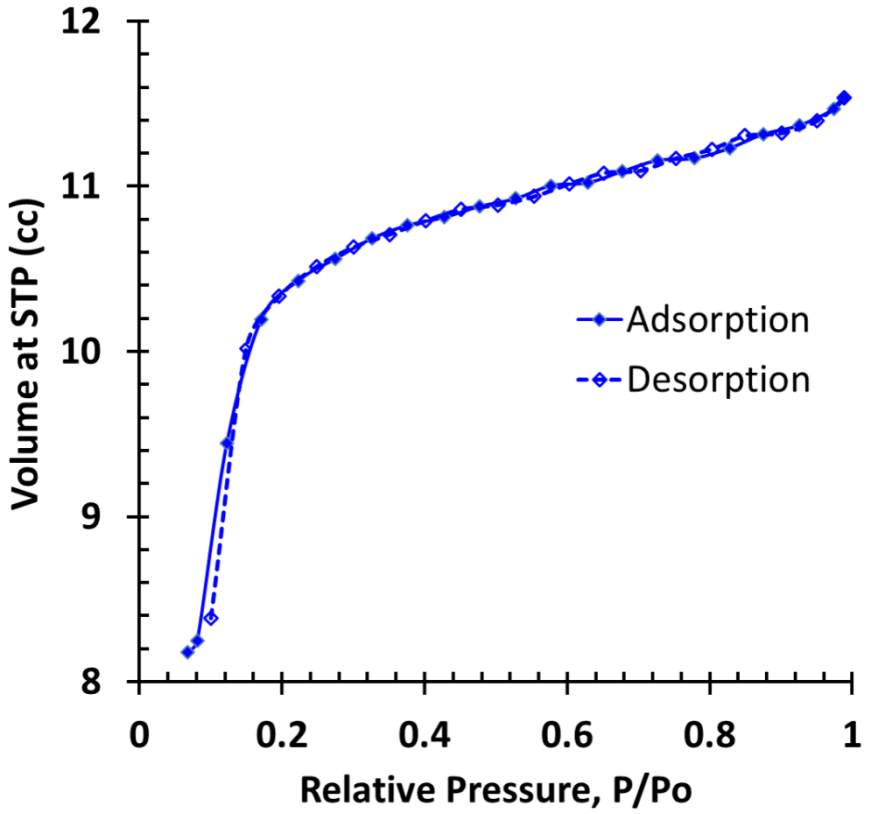

Figure S6. Single component adsorption isotherms (solid symbols) and desorption isotherms (open symbols) of N_2 in SBMOF-2 collected at 77 K.

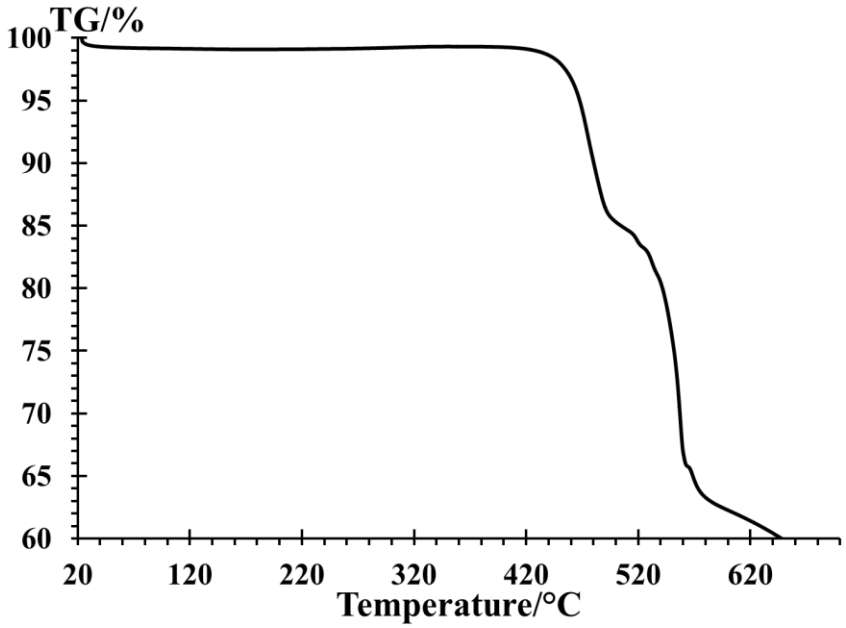

Figure S7. TGA plot of SBMOF-2 after exposing to air for 5 days.

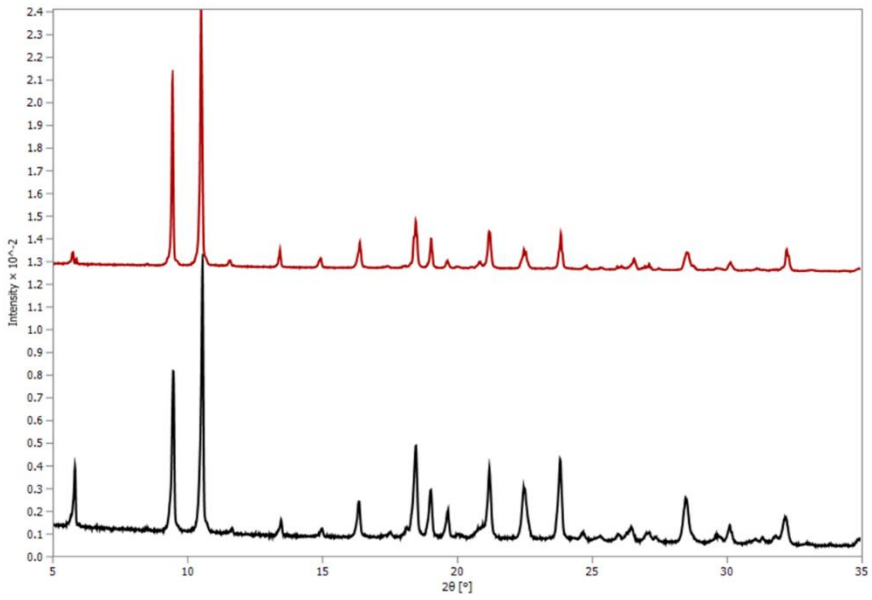

Figure S8. PXRD patterns of SBMOF-2 (black) and SBMOF-2 exposed to 100% humidity conditions for 5 days (red).

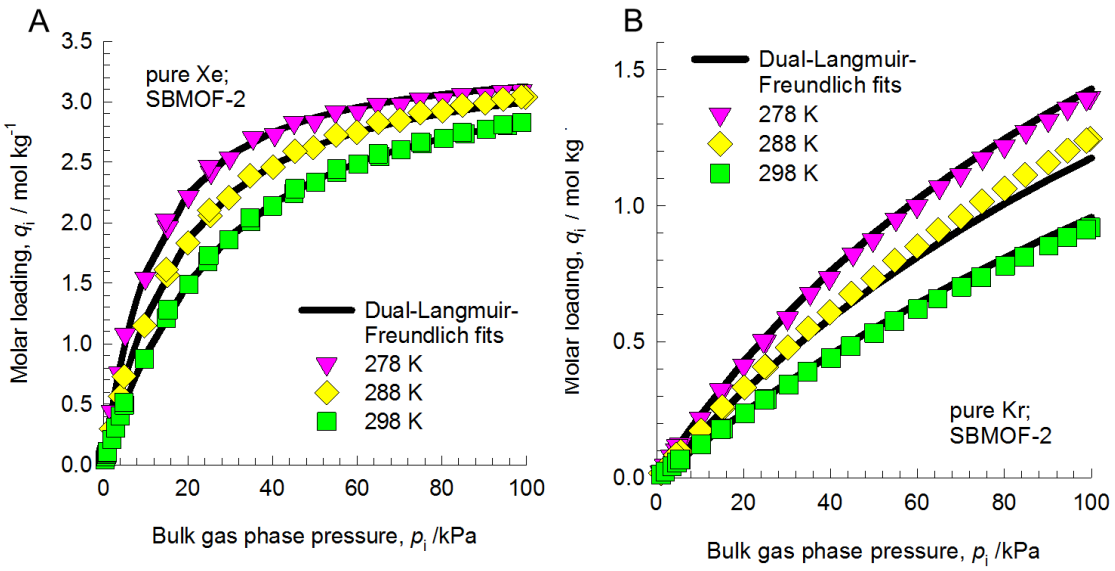

Figure S9. Comparison of the pure component isotherm data for (A) Xe, (B) Kr in SBMOF-2 with the fitted isotherms (shown by continuous solid lines) at 278 K, 288 K, and 298 K. The Langmuir-Freundlich fit parameters are provided in Table S2.

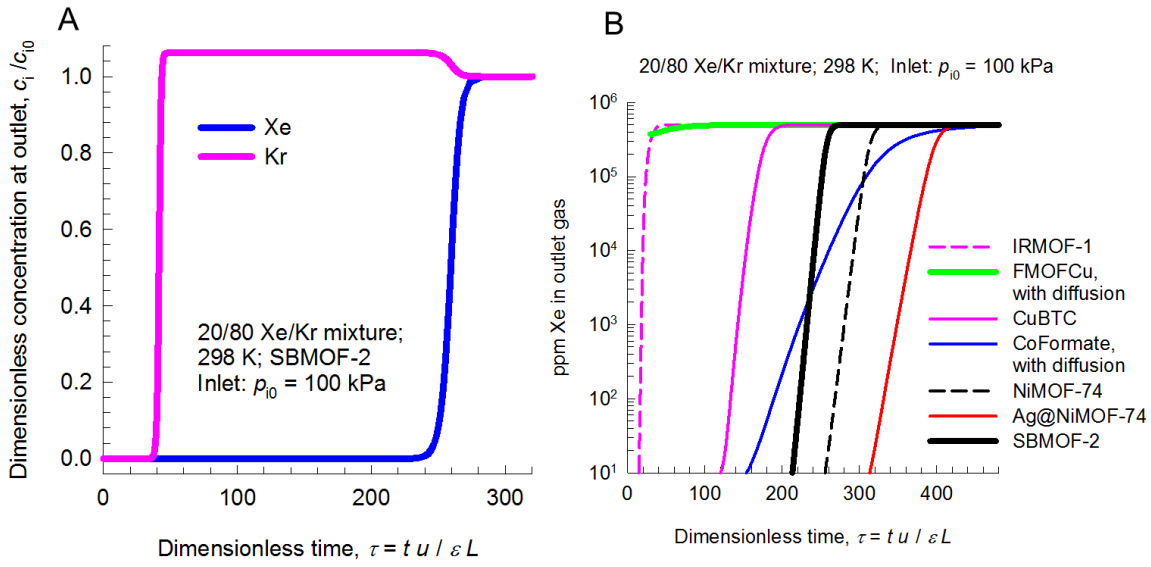

Figure S10. (A) Breakthrough characteristics of 20/80 Xe/Kr mixtures in fixed beds packed with SBMOF-2, operating at 100 kPa at 298 K. For the breakthrough simulations reported here we use the parameter values: L = 0.3 m; voidage of bed, ε = 0.4; interstitial gas velocity, v = 0.1 m/s; superficial gas velocity, u = 0.04 m/s. (B) The ppm Xe in the outlet gas mixture with feed gas of 20/80 Xe/Kr in fixed beds packed with SBMOF-2 and comparison with other compounds.[7]

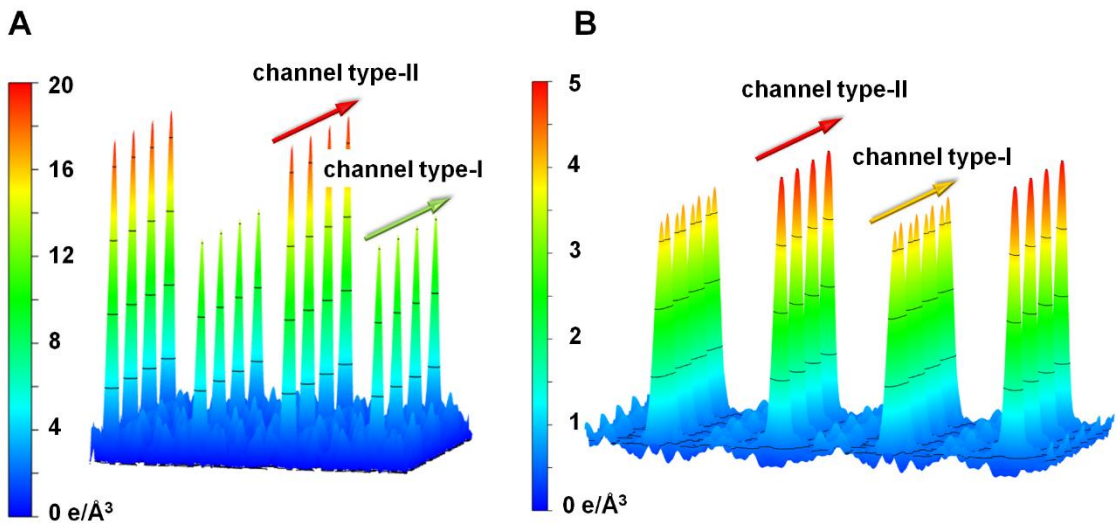

Figure S11. (A) 3D electron-density distribution map derived from single crystal XRD data for SBMOF-2:Xe. Contours are plotted with an interval of 4e/Å^3. (F) 3D electron-density distribution map derived from single crystal XRD data for SBMOF-2:Kr. Contours are plotted with an interval of 1.0 e/Å^3.

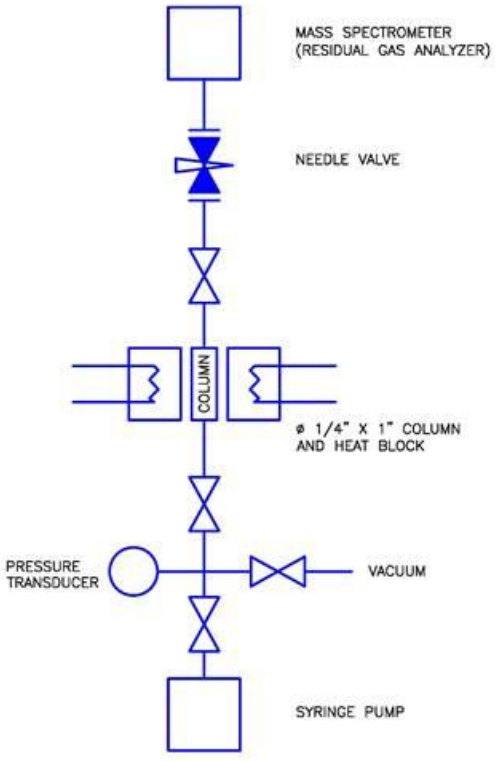

Figure S12. Schematic diagram of breakthrough analysis coupled with residual gas analyzer.

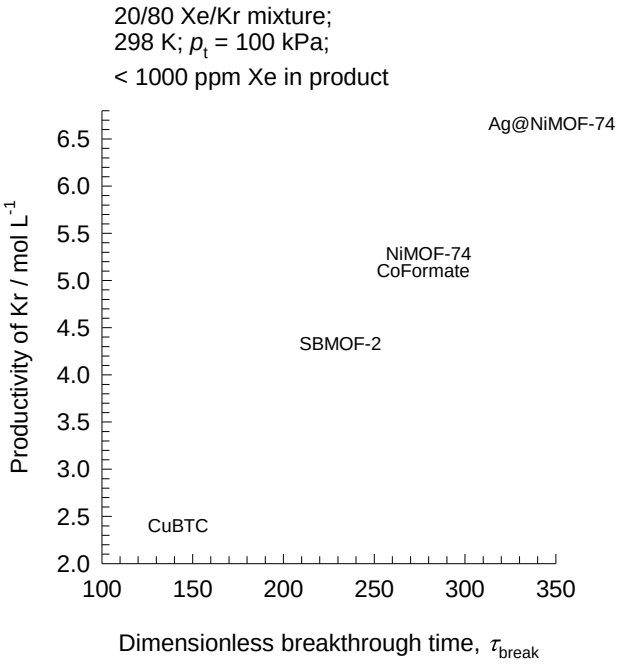

Figure S13. Dependence of the productivity of pure Kr (with < 1000 ppm < Xe), expressed in mol of product per L of MOF, as a function of the dimensionless breakthrough time, τ_{break}.

Table S1 Crystallographic data of as-synthesized, activated, Xe and Kr loaded SBMOF-2

	As-synthesized	Activated	Xe loaded	Kr loaded
Empirical formula	$CaC_{34}H_{20}O_{10.66}$	$CaC_{34}H_{20}O_8$	$CaC_{34}H_{20}O_8 \cdot Xe_{1.45}$	$CaC_{34}H_{20}O_8 \cdot Kr_{0.51}$
T/K	293(2)	100(2)	100(2)	100(2)
λ (Å)	0.71073	0.71073	1.54184	1.54184
a (Å)	5.1594(2)	5.1011(3)	5.1812(3)	5.1161(3)
b (Å)	11.0274(6)	10.8715(9)	10.7420(6)	10.8239(4)
c (Å)	15.2740(8)	15.2363(8)	15.1224(6)	15.2598(4)
α (°)	83.310(4)	83.132(5)	82.466(4)	82.990(2)
β (°)	87.657(4)	85.982(4)	84.928(4)	85.885(3)
γ (°)	83.128(4)	83.032(5)	82.691(5)	83.050(4)
Volume($Å^3$)	856.57(7)	831.37(10)	825.41(7)	832.16(6)
$Density_{cacl}$(g/cm^3)	1.239	1.192	1.583	1.277
Mu (mm^{-1})	0.238	0.235	13.489	2.831
Reflections, unique	3502	4125	3377	3525
Reflections, observed[$I>2\sigma(I)$]	2610	2894	2731	3074
R_{int}	0.0479	0.0815	0.0481	0.0581
Completeness to θ_{max}	0.998	0.999	0.996	0.992
F(000)	329	308	386	326
Goodness of fit	0.895	1.018	1.03	1.067
Data/restraints/parameter	3502/1/216	4125/0/196	3377/0/210	3525/0/210
R_1[$I>2\sigma(I)$]	0.0440	0.0523	0.0423	0.0483
R_1[all data]	0.0657	0.0854	0.0568	0.0562
wR_2 [all data]	0.1242	0.1358	0.1112	0.1328

Table S2 Dual-Langmuir-Freundlich parameters for adsorption of Xe and Kr in SBMOF-2.

	Site A				Site B			
	$q_{A,sat}$ mol kg^{-1}	b_{A0} Pa$^{-\nu_i}$	E_A kJ mol^{-1}	ν_A dimensionless	$q_{B,sat}$ mol kg^{-1}	b_{B0} Pa$^{-\nu_i}$	E_B kJ mol^{-1}	ν_B dimensionless
Xe	0.23	2.54×10^{-9}	29.3	0.95	3.13	1.12×10^{-11}	32.2	1.2
Kr	1.73	5.52×10^{-11}	20.3	1.2	1.81	4.66×10^{-10}	23.4	1

IV. References

(1) Sheldrick, G. M. *Acta Crystallogr. A* **1990**, 46, 467.
(2) Sheldrick, G. M. *SHELXL-97* (University of Göttingen, **1997**).
(3) Myers, A. L.; Prausnitz, J. M. *A.I.Ch.E.J.* **1965**, 11, 121.
(4) Krishna, R.; Long, J. R. *J. Phys. Chem. C* **2011**, 115, 12941.
(5) Krishna, R. *Micropor Mesopor Mat* **2014**, 185, 30.
(6) Wang, H.; Yao, K.; Zhang, Z.; Jagiello, J.; Gong, Q.; Han, Y.; Li, J. *Chem. Sci.* 2**014**,5, 620
(7) Banerjee, D.; Cairns, A. J.; Liu, J.; Motkuri, R. K.; Nune, S. K.; Fer-nandez, C. A.; Krishna, R.; Strachan, D. M.; Thallapally, P. K. *Acc. Chem. Res*. **2015**, 48(2), 211.